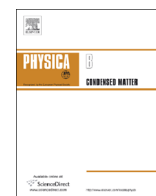




ELSEVIER

Contents lists available at ScienceDirect

Physica B

journal homepage: [www.elsevier.com/locate/physb](http://www.elsevier.com/locate/physb)

# Enhancement of resistive switching effect in double-layered Pt/Pr<sub>0.7</sub>Ca<sub>0.3</sub>MnO<sub>3</sub>/La<sub>0.6</sub>Pr<sub>0.4</sub>MnO<sub>3</sub>/SrNb<sub>0.01</sub>Ti<sub>0.99</sub>O<sub>3</sub> heterostructure

Yu-ling Jin, Zhong-tang Xu, Kui-juan Jin\*, Xu He, Can Wang, Hui-bin Lu

Beijing National Laboratory for Condensed Matter Physics, Institute of Physics, Chinese Academy of Sciences, Beijing 100190, China

## ARTICLE INFO

### Article history:

Received 12 November 2013

Received in revised form

1 March 2014

Accepted 29 April 2014

Available online 15 May 2014

### Keywords:

Perovskite oxide

Heterostructure

Oxygen vacancy

Resistive switching

## ABSTRACT

Resistive switching (RS) effect in the double-layered structure of Pt/Pr<sub>0.7</sub>Ca<sub>0.3</sub>MnO<sub>3</sub> (PCMO)/La<sub>0.6</sub>Pr<sub>0.4</sub>MnO<sub>3</sub> (LPMO)/SrNb<sub>0.01</sub>Ti<sub>0.99</sub>O<sub>3</sub> (SNTO) are improved comparing with that in the single-layered structure of Pt/PCMO/SNTO. We propose that the RS characteristics of the two structures depend on the electronic properties of the depletion layer formed in PCMO layer with negative space-charge near the interface of PCMO and LPMO (or SNTO), which should be caused by the migration of oxygen vacancies. Our numerical results show that the negative space-charge region formed in the whole LPMO layer in Pt/PCMO/LPMO/SNTO causes an increase of the electric field, which results in the increase of the number of oxygen vacancies to migrate and thereby improving the RS effect.

© 2014 Published by Elsevier B.V.

## 1. Introduction

The resistive switching (RS) phenomenon has been found in a wide variety of perovskite oxides like manganites, titanates and zirconates with metal-insulator-metal structures [1–3]. Several theoretical models have been proposed to explain the RS behavior, such as the modulation of the Schottky barrier [4,5], filamentary conducting path [6], electrochemical migration of oxygen vacancies [7–11] and oxidation/reduction reaction [12–14]. RS effect receives more attention in the recent 50 years because it holds immense potential for a next-generation nonvolatile memories with high density, great scalability and low power consumption [15,16]. The ratio of the resistance at high-resistance state (HRS) to the resistance at low-resistance state (LRS), which is expressed by  $R_H/R_L$ , is an important property in application. To increase the resistance ratio and also improve the endurance behavior of RS effect of oxides, recent works have mainly focused on three influencing factors, the type of the electrode materials [8,14], the concentration of oxygen vacancies in the sample [17,18] and the structure of the device [19–22]. The type of interface contact, which is related to the work function of the electrode, plays an important role in the RS effect. It is also found that the electrochemistry reaction of metal electrode could improve the RS characteristics [12,14]. In our recent work, we have investigated the role of oxygen vacancies and reported that the increasing of the density of oxygen vacancies in a certain range could increase

the resistance ratio of LaMnO<sub>3</sub> films. In the aspect of structure design, the certain multilayer structure is found to possess the improved RS characteristics compared with single-layered structure.

In recent years, the RS effect in Pr<sub>0.7</sub>Ca<sub>0.3</sub>MnO<sub>3</sub> (PCMO) sandwich structures have attracted great attention due to its larger resistance value than that of bulk crystal and simple structure [23]. The migration of oxygen vacancies at the interface between PCMO film and the metallic electrode is considered to play a crucial role in the RS process. Nian et al. explained the resistive switching effect of PCMO by considering the movement of oxygen vacancies at the interface [9]. Asanuma et al. reported the resistive switching effect originated from the change of the band diagrams of the Ti/PCMO junctions due to the migration of the oxygen ions [10].

In this paper, we investigate the RS effect with improved hysteresis behavior in multilayer structure of Pt/PCMO/La<sub>0.6</sub>Pr<sub>0.4</sub>MnO<sub>3</sub> (LPMO)/SrNb<sub>0.01</sub>Ti<sub>0.99</sub>O<sub>3</sub> (SNTO) comparing with that in the single-layered structure of Pt/PCMO/SNTO. In addition, to verify the role of the LPMO layer, a double-layered structure of Pt/LPMO/PCMO/SNTO was also fabricated. The experiment results show that the resistive switching effect in Pt/LPMO/PCMO/SNTO is weaker than that of Pt/PCMO/LPMO/SNTO. We also provide some numerical results for the understanding of the RS behavior.

## 2. Experiments

Three types of samples made of PCMO, LPMO/PCMO, and PCMO/LPMO films were fabricated on the SNTO (0 0 1) substrates with 3 × 5 mm<sup>2</sup> large and 0.5 mm thickness by laser molecular

\* Corresponding author. Tel.: +86 10 82648099.

E-mail address: [kjin@iphy.ac.cn](mailto:kjin@iphy.ac.cn) (K.-j. Jin).

beam epitaxy (MBE), which is with a pulsed XeCl excimer laser beam ( $\sim 20$  ns, 2 Hz,  $\sim 1.5$  J/cm<sup>2</sup>) focused on the sintered ceramic PCMO and LPMO targets. The oxygen pressure was kept  $5 \times 10^{-2}$  Pa during the deposition and the substrate temperature detected by an infrared pyrometer was around 570 °C. The thickness of the PCMO and LPMO are about 100 nm and 6 nm, respectively. Finally, the Pt top electrode (TE) in a diameter of 100  $\mu$ m was deposited and patterned with a metal mask. The crystalline structures of the samples were examined by X-ray diffraction (XRD). The XRD results demonstrate that the films are epitaxially grown along the *c*-axis with single phase. The current–voltage (*I*–*V*) behaviors were measured by a Keithley 2400 source meter at room temperature. The forward-bias is defined by the positive voltage applied on the TE Pt.

### 3. Results and discussions

Fig. 1(a) shows that the experimental *I*–*V* characteristics of the Pt/PCMO/SNTO, Pt/LPMO/PCMO/SNTO and Pt/PCMO/LPMO/SNTO structures exhibit bipolar resistive switching behaviors. The bias voltage was applied on the TE Pt in the direction of  $0 \text{ V} \rightarrow -2 \text{ V} \rightarrow 0 \text{ V} \rightarrow 3 \text{ V} \rightarrow 0 \text{ V}$ . The resistances of the structures are switched from LRS to HRS after the forward-bias scan. In order to avoid the

dielectric breakdown, the maximum of negative-bias is only  $-2.0$  V. Thus, the resistive switching behavior is not obvious under the reverse-bias.

PCMO is a p-type semiconductor with the work function  $\sim 4.9$  eV measured by ultraviolet photoelectron spectroscopy (UPS). SNTO is a highly doped n-type semiconductor as the bottom electrode. Since the work function of Pt and SNTO are about 5.6 eV and 4.05 eV, respectively, the p–n heterojunction is formed at the interface of PCMO/SNTO, while the ohmic contact would appear at the interface of Pt/PCMO. The obvious rectifying property of Pt/PCMO/SNTO is attributed to the PCMO/SNTO heterojunction. The contact resistance of the PCMO/SNTO dominates the *I*–*V* characteristics. Oxygen vacancies are inevitable in the PCMO layer because of the low oxygen pressure  $5 \times 10^{-2}$  Pa during the deposition. Oxygen vacancies act as effective donors after releasing one or two electrons into the conduction band and become positively charged, which was confirmed by Hall measurement [17].

The migration of the oxygen vacancies at the interface under the electric field is considered to play a crucial role in the RS phenomenon. The RS process is corresponding to the switch of the contact resistance at interfaces, which is mainly attributed to the depletion layer formed in PCMO with negative space-charge at the PCMO/SNTO interface. When the positive voltage applied on the TE, the positively charged oxygen vacancies migrate from the bulk of PCMO to the interface of PCMO/SNTO. The increase of the number of oxygen vacancies near the interface of PCMO/SNTO results in decreasing of the density and mobility of the holes, because oxygen vacancies act as donor impurities [24,25]. The band gap in the PCMO side would be enlarged, because of the decrease of the one-electron  $e_g$  band width due to the increase of the concentration of oxygen vacancies, which is also confirmed by the experiments [10,25]. Thus, the width of depletion layer in PCMO increases. The contact resistance of p–n junction, which contributes to the major part of the whole resistance of the device, increases accordingly. Eventually, the resistance of the device is switched from LRS to HRS. In addition, electric Joule heating is an unavoidable factor that might affect the RS performance in these structures during measurements. Because Joule heating is mainly responsible for the unipolar RS effect, in our case Joule heating is not the dominant mechanism [26,27]. To minimize the heating effect, we stopped for two minutes after each point measurement.

In order to improve the RS effect of Pt/PCMO/SNTO, a LPMO thin film (about 6 nm) was deposited on the SNTO substrate to form a double-layered Pt/PCMO/LPMO/SNTO structure. The *I*–*V* curves in Fig. 1(a) show that the Pt/PCMO/LPMO/SNTO structure performs the most pronounced hysteresis behavior. Moreover, Fig. 1(b) shows the resistance ratio  $R_H/R_L$  of the structures under pulse voltage of  $\pm 5$  V with the width of 5  $\mu$ s, 10  $\mu$ s, 50  $\mu$ s, 100  $\mu$ s, 250  $\mu$ s, 0.5 ms, 1 ms and 5 ms, respectively. When the pulse width is 5 ms, the resistance ratios  $R_H/R_L$  are 41.1, 5.2 and 2.5 of Pt/PCMO/LPMO/SNTO, Pt/LPMO/PCMO/SNTO and Pt/PCMO/SNTO, respectively. As we expected, the resistance ratio of Pt/PCMO/LPMO/SNTO structure became larger than that of Pt/PCMO/SNTO and Pt/LPMO/PCMO/SNTO. The switching time is about millisecond scale, which may be due to the electret effect [28,29].

In the LPMO film the Pr ions are in mixed-valence states of Pr<sup>4+</sup> and Pr<sup>3+</sup> [30]. LPMO is most likely a low electron-doping manganite [31]. Thus the p–n heterojunction barrier and n–n heterojunction barrier are expected to form at PCMO/LPMO and LPMO/SNTO interfaces, respectively. The mechanism of the RS effect of double-layered structure of Pt/PCMO/LPMO/SNTO is more complex.

In order to investigate the mechanism of RS effect of Pt/PCMO/LPMO/SNTO, we carried out a theoretical calculation on the transport properties of the structure with double barriers by self-consistently solving the Poisson and carrier continuity

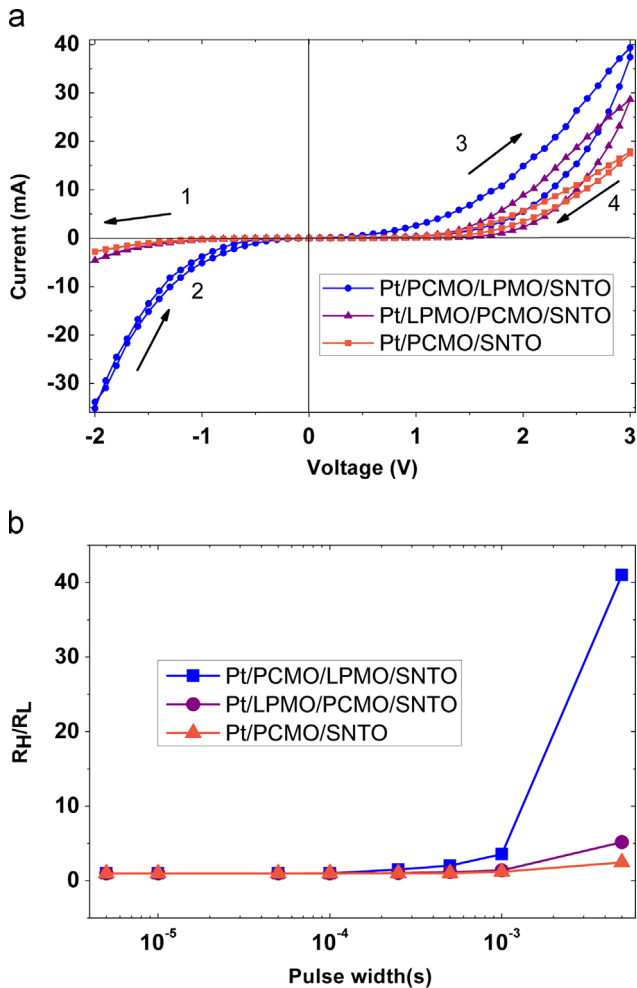


Fig. 1. (a) The measured *I*–*V* characteristics of Pt/PCMO/SNTO, Pt/PCMO/LPMO/SNTO and Pt/LPMO/PCMO/SNTO structures. (b) The resistance ratio  $R_H/R_L$  of Pt/PCMO/LPMO/SNTO, Pt/LPMO/PCMO/SNTO and Pt/PCMO/SNTO structures under the pulse voltage of  $\pm 5$  V with the width of 5  $\mu$ s, 10  $\mu$ s, 50  $\mu$ s, 100  $\mu$ s, 250  $\mu$ s, 0.5 ms, 1 ms and 5 ms, respectively.

equations.

$$\frac{\partial^2 \psi(x)}{\partial x^2} = -\frac{q}{\epsilon_r \epsilon_0} (p(x) - n(x) + N(x)), \quad (1)$$

$$\frac{\partial p(x)}{\partial t} = -\frac{1}{q} \frac{\partial J_p(x)}{\partial x} - U(x), \quad (2)$$

$$\frac{\partial n(x)}{\partial t} = \frac{1}{q} \frac{\partial J_n(x)}{\partial x} - U(x), \quad (3)$$

where  $\psi(x)$  is the electrostatic potential.  $n(x)$  and  $p(x)$  are the concentration of electrons and holes, respectively.  $N(x)$  is doping concentration.  $U(x)$  is the recombination rate of the Shockley–Read–Hall recombination process [32–35].  $q$ ,  $\epsilon_r$  and  $\epsilon_0$  denote the electron charge, dynamic dielectric constant and permittivity of free space, respectively.  $J_n(x)$  and  $J_p(x)$  are the current density of electrons and holes, respectively:

$$J_n(x) = -qu_n n(x) \frac{\partial \phi_n(x)}{\partial x}, \quad (4)$$

$$J_p(x) = -qu_p p(x) \frac{\partial \phi_p(x)}{\partial x}, \quad (5)$$

where  $\phi_n(x)$  and  $\phi_p(x)$  are the quasi Fermi potential of electrons and holes, respectively.  $\mu_n$  and  $\mu_p$  represent the mobility of the electrons and holes, respectively. The concentration distribution of the electrons and holes are in the relation with  $\phi_n(x)$  and  $\phi_p(x)$ , respectively:

$$n(x) = n_i \exp\left(\frac{q}{kT}(\psi(x) - \phi_n(x))\right), \quad (6)$$

$$p(x) = n_i \exp\left(\frac{q}{kT}(\phi_p(x) - \psi(x))\right), \quad (7)$$

where  $n_i$ ,  $k$  and  $T$  denote the intrinsic carrier concentration, the Boltzmann constant and the temperature. Richardson thermionic current based on the thermionic–emission–diffusion theory [36] is employed as the current boundary condition. The current density  $J_n(x_i)$  and  $J_p(x_i)$  across the interface of the heterojunction  $x_i$  are given as follows:

$$J_n(x_i) = -A_{n-}^* T^2 \exp\left(-\frac{|\Delta E_c|}{kT} \theta(\Delta E_c)\right) n(x_i - 0) + A_{n+}^* T^2 \exp\left(-\frac{|\Delta E_c|}{kT} \theta(-\Delta E_c)\right) n(x_i + 0), \quad (8)$$

$$J_p(x_i) = A_{p-}^* T^2 \exp\left(-\frac{|\Delta E_v|}{kT} \theta(-\Delta E_v)\right) p(x_i - 0) - A_{p+}^* T^2 \exp\left(-\frac{|\Delta E_v|}{kT} \theta(\Delta E_v)\right) p(x_i + 0), \quad (9)$$

where  $A^* n - (A^* p -)$  and  $A^* n + (A^* p +)$  are the Richard constants of electrons (hole) in the left and right sides of the heterojunction, respectively.  $\Delta E_c$  ( $\Delta E_v$ ) denotes the difference between bottom of conductive band (top of valence band) in left and right region.  $\theta(x)$  is the step function: if  $x < 0$ ,  $\theta(x) = 0$ ; else if  $x \geq 0$ ,  $\theta(x) = 1$ . Moreover, the tunneling current density of electrons is included in our calculation. Eqs. (1–3) coupled with the boundary conditions (8) and (9) are solved self-consistently using the numerical method. The standard finite difference method is utilized to discretize these equations. Thus, the three primary variables the electrostatic potential  $\psi(x)$ , the quasi Fermi potential of electrons  $\phi_n(x)$ , and the quasi Fermi potential of holes  $\phi_p(x)$  are obtained using the iterative technique. Because of the low doping density of LPMO film and the strong electron injection from the SNT0, the transport characteristics of LPMO might be governed by the space charge limited conduction mechanism in the simulation model.

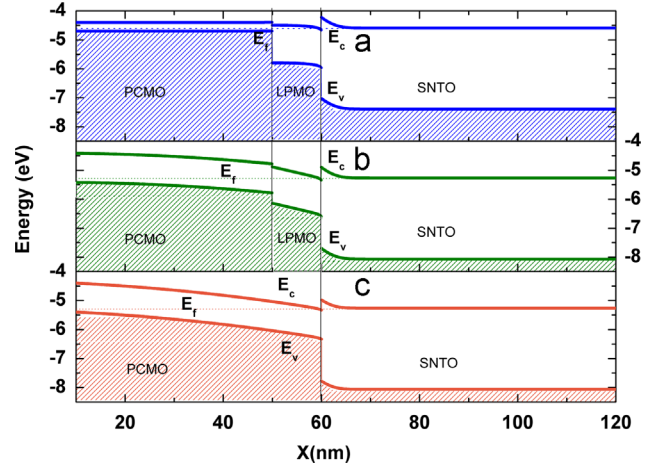


Fig. 2. The energy band by numerical calculation of (a) Pt/PCMO/LPMO/SNT0 at LRS, (b) at HRS, and (c) Pt/PCMO/SNT0 structures under 0 V.

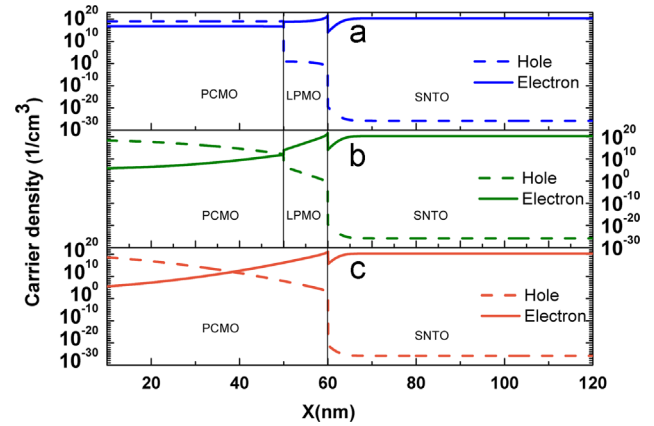


Fig. 3. The carrier distribution by numerical calculation of (a) Pt/PCMO/LPMO/SNT0 at LRS, (b) at HRS, and (c) Pt/PCMO/SNT0 structures under 0 V.

Fig. 2 shows the band diagrams of Pt/PCMO/SNT0 and Pt/PCMO/LPMO/SNT0 at LRS and HRS under 0 V by calculation. The depletion layer with negative space-charge is formed in PCMO near the interface of PCMO/LPMO in the double-layered structure Pt/PCMO/LPMO/SNT0. Because the carrier density in LPMO is very small, electrons would be injected from SNT0 to LPMO. The calculation results show the whole LPMO layer all became negative space-charge layer due to the small thickness and low doping density. The distribution of carrier density of Pt/PCMO/SNT0 and Pt/PCMO/LPMO/SNT0 at LRS and HRS under 0 V obtained by numerical calculation is plotted in Fig. 3. The distribution of the density of net charge, which composes of the free carrier and ionized acceptor, is shown in Fig. 4. The negative space-charge region is formed in PCMO depletion layer near the interface of PCMO/LPMO and the whole LPMO layer. When the positive voltage is applied on the TE Pt, oxygen vacancies transport from the bulk of PCMO to the interface of PCMO/LPMO. The corresponding schematic diagram is shown in Fig. 4. The barrier height of the heterojunction decreases slightly, but the width of the depletion region becomes distinctly larger at the HRS, because oxygen vacancies are repelled to the interface of PCMO/LPMO, which can be seen from the band diagram by calculation in Fig. 2. Thus, the contact resistance increases and thereby the whole structure is switched from LRS to HRS.

The double-layered structure of Pt/PCMO/LPMO/SNT0 has more pronounced RS than that of Pt/PCMO/SNT0, which is supposed to attribute to the more substantial change of the contact resistance of

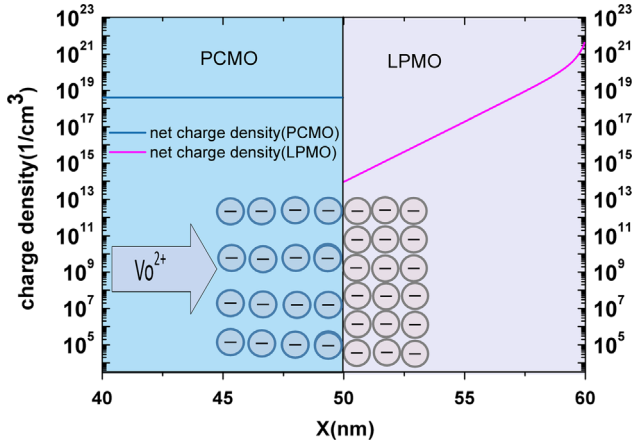


Fig. 4. The schematic of the migration of oxygen vacancies in the negative space-charge region. The solid line is the negative net charge density in PCMO and LPMO by calculating.

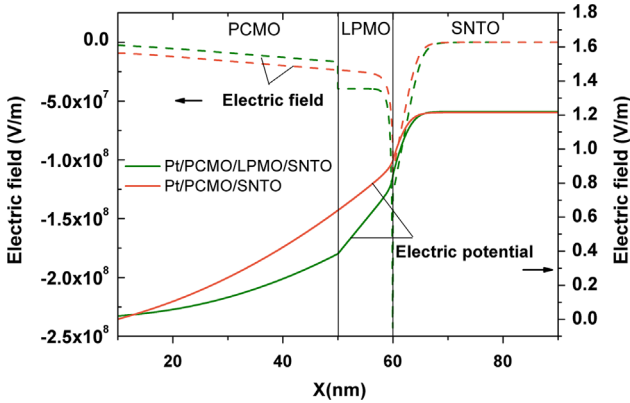


Fig. 5. The distribution of electric field and potential of Pt/PCMO/LPMO/SNTO structure compared with that of Pt/PCMO/SNTO structure at HRS under 0 V.

PCMO/LPMO under the external voltage. We compare the electric field distribution obtained by numerical calculation of Pt/PCMO/SNTO and Pt/PCMO/LPMO/SNTO structures under 0 V shown in Fig. 5. The completely depleted LPMO layer increases the electric field strength, which could be explained by the differences in dielectric constants of PCMO ( $\sim 190\epsilon_0$ ), of LPMO ( $\sim 40\epsilon_0$ ), and of SNTO ( $\sim 150\epsilon_0$ ) obtained by our measurement [37]. The increasing of the electric field, which is in the same direction with the migration of oxygen vacancies, would increase the force which binds the oxygen vacancies at the interface. The contact resistance of PCMO/LPMO heterojunction in Pt/PCMO/LPMO/SNTO changes more significantly than that of PCMO/SNTO in Pt/PCMO/SNTO. So the resistive switching effect in Pt/PCMO/LPMO/SNTO is more prominent than that in Pt/PCMO/SNTO under the forward-bias. The  $I$ - $V$  curves of Pt/PCMO/SNTO and Pt/PCMO/LPMO/SNTO at LRS and HRS obtained by numerical calculation are plotted in Fig. 6. Because Pt/PCMO/SNTO structure exhibits no obvious hysteresis behavior, we only plotted the HRS of it. The calculated results of the transport characteristics of Pt/PCMO/LPMO/SNTO structure at the HRS and LRS are consistent with the experimental ones shown in Fig. 1(a). The parameters used for calculation are listed in Table 1.

To verify the assumption, we also fabricated the Pt/LPMO/PCMO/SNTO structure. When LPMO film is on the top of PCMO, holes will diffuse into the LPMO from PCMO due to the concentration gradient. Because the positive charge region formed in LPMO can also assist the oxygen vacancies to migrate from PCMO bulk to the interface of PCMO/SNTO, the RS characteristics is improved

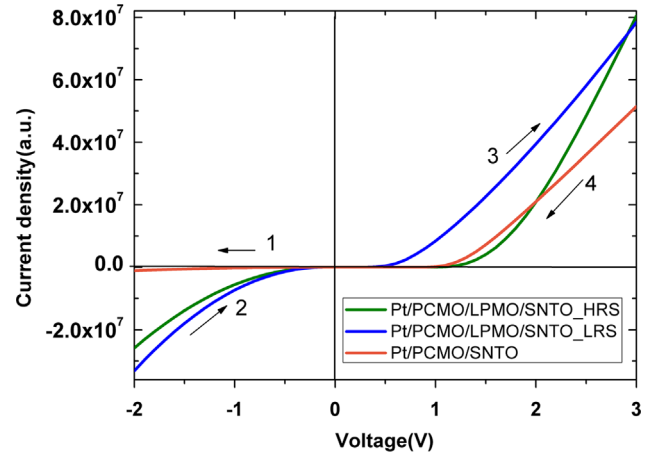


Fig. 6. The calculated  $I$ - $V$  characteristics of Pt/PCMO/SNTO and Pt/PCMO/LPMO/SNTO structures.

Table 1  
Parameters used in calculation.

| Material parameter  | Pt/PCMO/LPMO/SNTO LRS | Pt/PCMO/LPMO/SNTO HRS | Pt/PCMO/SNTO         |
|---|-----------------------|-----------------------|----------------------|
| Doping concentration of PCMO ( $\text{cm}^{-3}$ )                   | $1.0 \times 10^{19}$  | $4.0 \times 10^{18}$  | $4.0 \times 10^{18}$ |
| Hole mobility of PCMO ( $\text{cm}^2 \text{V}^{-1} \text{s}^{-1}$ ) | 15 <sup>a</sup>       | 13                    | 13                   |
| Band gap of PCMO (eV)   | 0.3 <sup>b</sup>      | 1.0                   | 1.0                  |
| Band gap of LPMO (eV)   | 1.3                   | 1.26                  | –                    |

<sup>a</sup> Parameter taken from Ref. [38]

<sup>b</sup> Parameter taken from Ref. [39]

comparing with the single-layered structure. However, the resistive switching effect is weaker than that of Pt/PCMO/LPMO/SNTO structure measured in the same condition shown in Fig. 1. The RS characteristics in Pt/PCMO/LPMO/SNTO and Pt/LPMO/PCMO/SNTO mainly depend on the variation of depletion layer width in PCMO at the interfaces of PCMO/LPMO and PCMO/SNTO under forward-bias. When PCMO is on the top of PCMO, it cannot make as large effect on the migration of oxygen vacancies in the PCMO as that when it located between PCMO and SNTO. So the electronic properties of the depletion layer of PCMO in Pt/LPMO/PCMO/SNTO are altered less than that in Pt/PCMO/LPMO/SNTO. Therefore, it is speculated that the RS effect can be improved by adopting a lower doped thin film with smaller dielectric constant than that of the oxide film particularly at the interface of the depletion layer. The larger the electric properties of that interface changed, the larger the hysteresis behavior and the RS effect can be.

#### 4. Conclusions

In summary, we proposed that the migration of the oxygen vacancies is responsible for the RS effect. We have improved the RS effect of Pt/PCMO/SNTO structure by adopting the LPMO layer between the PCMO layer and SNTO substrate. The negative charge region is formed in LPMO layer, which could assist more oxygen vacancies to migrate and change the electronic properties of the interface more significantly. Therefore, the resistive switching effect is enhanced accordingly. To verify the role of played by LPMO layer, we also fabricated the double-layered structure of Pt/LPMO/PCMO/SNTO, which exhibits weaker hysteresis behavior than that of Pt/PCMO/LPMO/SNTO. The theoretical model is carried out to explain the role of the oxygen vacancies and the LPMO layer

in detail. The transport characteristics of the Pt/PCMO/LPMO/SNTO with double heterojunctions are also obtained by numerical calculation. The results present in this paper should be helpful for the understanding of the RS properties in the multilayer structures, as well as for the further designing of the multilayer structures.

### Acknowledgments

This work was supported by the National Basic Research Program of China (Nos. 2012CB921403 and 2013CB328706) and the National Natural Science Foundation of China (Nos. 10825418 and 11134012).

### References:

- [1] T. Keiver, U. Bottger, C. Schindler, R. Waser, *Appl. Phys. Lett.* 91 (2007) 083506.
- [2] A. Beck, J. Bednorz, C. Gerber, C. Rossel, D. Widmer, *Appl. Phys. Lett.* 77 (2000) 139.
- [3] S. Liu, N. Wu, A. Ignatiev, *Appl. Phys. Lett.* 76 (2000) 2749.
- [4] J.J. Yang, M.D. Pickett, X. Li, D.A. Ohlberg, D.R. Stewart, R.S. Williams, *Nat. Nanotechnol.* 3 (2008) 429.
- [5] H. Shima, N. Zhong, H. Akinaga, *Appl. Phys. Lett.* 94 (2009) 082905.
- [6] K. Kinoshita, H. Noshiro, C. Yoshida, Y. Sato, M. Aoki, Y. Sugiyama, *J. Mater. Res.* 23 (2008) 812.
- [7] R. Waser, R. Dittmann, G. Staikov, K. Szot, *Adv. Mater.* 21 (2009) 2632.
- [8] A. Sawa, *Mater. Today* 11 (2008) 28.
- [9] Y.B. Nian, J. Strozier, N.J. Wu, X. Chen, A. Ignatiev, *Phys. Rev. Lett.* 98 (2007) 146403.
- [10] S. Asanuma, H. Akoh, H. Yamada, A. Sawa, *Phys. Rev. B* 80 (2009) 235113.
- [11] B. Bryant, C. Renner, Y. Tokunaga, Y. Tokura, G. Aeppli, *Nat. Commun.* 2 (2011) 212.
- [12] W. Shen, R. Dittmann, U. Breuer, R. Waser, *Appl. Phys. Lett.* 93 (2008) 222102.
- [13] R. Yang, X. Li, W. Yu, X. Gao, D. Shang, X. Liu, X. Cao, Q. Wang, L. Chen, *Appl. Phys. Lett.* 95 (2009) 072105.
- [14] C. Dong, D. Shang, L. Shi, J. Sun, B. Shen, F. Zhuge, R. Li, W. Chen, *Appl. Phys. Lett.* 98 (2011) 072107.
- [15] R. Waser, M. Aono, *Nat. Mater.* 6 (2007) 833.
- [16] J.J. Yang, D.B. Strukov, D.R. Stewart, *Nat. Nanotechnol.* 8 (2012) 13.
- [17] Z.T. Xu, K.J. Jin, L. Gu, Y.L. Jin, C. Ge, C. Wang, H.Z. Guo, H.B. Lu, R.Q. Zhao, G.Z. Yang, *Small* 8 (2012) 1279.
- [18] K.C. Liu, W.H. Tzeng, K.M. Chang, J.J. Huang, Y.J. Lee, P.H. Yeh, P.S. Chen, H.Y. Lee, F. Chen, M.J. Tsai, *Thin Solid Films* 520 (2011) 1246.
- [19] C. Cheng, A. Chin, F. Yeh, *Appl. Phys. Lett.* 98 (2011) 052905.
- [20] X. Liu, K.P. Biju, S. Park, W. Lee, D. Lee, K. Seo, H. Hwang, *Electrochem. Solid-State Lett.* 14 (2011) H9.
- [21] J.K. Lee, S. Jung, J. Park, S.W. Chung, J. Sung Roh, S.J. Hong, I. Hwan Cho, H. I. Kwon, C. Hyeong Park, B.G. Park, *Appl. Phys. Lett.* 101 (2012) 103506.
- [22] X. Liu, K.P. Biju, S. Park, I. Kim, M. Siddik, S. Sadaf, H. Hwang, *Current Appl. Phys.* 11 (2011) 58.
- [23] A. Sawa, T. Fujii, M. Kawasaki, Y. Tokura, *Appl. Phys. Lett.* 85 (2004) 4073.
- [24] M.L. Wilson, J.M. Byers, P.C. Dorsey, J.S. Horwitz, D.B. Chrisey, M.S. Osofsky, *J. Appl. Phys.* 81 (1997) 4971.
- [25] R. Mahesh, M. Itoh, *Solid State Ion.* 108 (1998) 201.
- [26] N. Biskup, A. de Andres, *Phys. Rev. B* 74 (2006) 184403.
- [27] A. Asamitsu, Y. Tomioka, H. Kuwahara, Y. Tokura, *Nature* 388 (1997) 50.
- [28] G. Sessler, M. Broadhurst, *Electrets*, Springer, New York, 1980.
- [29] J.F. Scott, C. Araujo, H.B. Meadows, L. McMillan, A. Shawabkeh, *J. Appl. Phys.* 66 (1989) 1444.
- [30] P. Duan, Z. Chen, S. Dai, L. Liu, J. Gao, J. Magn. *Magn. Mater.* 301 (2006) 521.
- [31] P. Duan, Z. Chen, S. Dai, Y. Zhou, H. Lu, K. Jin, B. Cheng, *Appl. Phys. Lett.* 84 (2004) 4741.
- [32] K. Horio, H. Yanai, *Electron devices*, *IEEE Trans.* 37 (1990) 1093.
- [33] K. Yang, J.R. East, G.I. Haddad, *Electron devices*, *IEEE Trans.* 41 (1994) 138.
- [34] P. Han, K.J. Jin, Y.L. Zhou, X. Wang, Z.s. Ma, S.F. Ren, A.G. Mal'shukov, K.A. Chao, *J. Appl. Phys.* 99 (2006) 074504.
- [35] K.H. Yang, J.R. East, G.I. Haddad, *Solid State Electron.* 36 (1993) 321.
- [36] S.F. Guo, *Solid State Electron.* 27 (1984) 537.
- [37] L. Liao, K.J. Jin, H.B. Lu, J. Qiu, P. Han, L.L. Zhang, *Physica Status Solidi A206*, 2009, 1655.
- [38] C.L. Hu, P. Han, K.J. Jin, H.B. Lu, G.Z. Yang, *J. Appl. Phys.* 103 (2008) 053701.
- [39] J. Dho, *Solid State Commun.* 150 (2010) 2243.